Mathematical Relationship of an Isotropic Point Source and the Spherically Distributed Antenna Array

Kristopher Buchanan[1], Timi Adeyemi[1], Carlos Flores-Molina[1], Sara Wheeland[1], and Steven Weiss[2]
[1]Space and Naval Warfare Systems Center Pacific (SSC Pacific): Electromagnetics Technology Branch, San Diego CA, USA
[2]Adelphi Laboratory Center: Antennas and RF Technology Integration Branch, 2800 Powder Mill Rd, Adelphi, MD 20783, USA

***Abstract*—This work investigates beam pattern behavior of an isotropic point source and a collection of sources distributed amongst a spherical volume. Pattern behavior is compared to the tapering of a plane wave expansion of spherical waves demonstrating self-adjoint characteristics. Beampatterns of atomic like orbitals and Zernike polynomials are provided as connections to common applications.**

***Index Terms*—Distributed beamforming.**

I. Introduction

Circular and spherical random arrays were first analyzed by Panicali and Lo mainly by using the variance, mean and correlation between elements [1]. A more insightful analysis was considered by [2] approximately a decade later with further examinations of circular [3]–[4] and spherical [5]–[10] array geometry.

This work presents a derivation of the exact and approximate array factor and mean-valued radiation pattern for spherically and circularly distributed random arrays from [11]–[12].

II. Formulation of the Exact Array Factor

The exact array factor can be shown as:

$$F\left(\theta,\phi\middle|R_n\right)=\frac{1}{N}\sum_{n=1}^{N}e^{jkR_n}=\frac{1}{N}\sum_{n=1}^{N}e^{jkr\sqrt{1+x^2-2x\cos\psi_n}},\ x=r_n/r \quad (1)$$
$$\cos\theta\equiv\cos\psi_n=\sin\theta\sin\theta_n\cos\left(\phi-\phi_n\right)+\cos\theta\cos\theta_n=\hat{r}\cdot\hat{r}_n$$

Since r is not a part of the integration it is placed into the term β (eqn. 4, [11]) such that $\beta = 2\pi\Delta fr/c$. Next, integration is done over the spherical volume of an isotropic point source located on the z axis by (2), and (3) [1]–[12]. Due to the change of variables ($x = r_n / r$) one obtains the multiplication of r^3 in (4), which reduces to (5) over its circularly symmetric ϕ integration:

$$\cos\theta\equiv\left(\cos\psi_n\middle|\theta_n=0°\right)=\hat{r}\cdot\hat{r}_n=\cos\theta, \quad (2)$$

$$\int_0^{r_n}\int_0^{\pi}\int_0^{2\pi}\exp\left[-j\beta\sqrt{1+\left(r_n/r\right)^2-2\left(r_n/r\right)\cos\theta}\right]r_n^2dr_n\sin\theta d\theta d\phi, \quad (3)$$

$$r^3\int_0^{A/r}\int_0^{\pi}\int_0^{2\pi}\exp\left[-j\beta\sqrt{1+x^2-2x\cos\theta}\right]x^2dxd\Omega, \quad (4)$$

$$2\pi r^3\int_0^{x'}\int_0^{\pi}\exp\left[-j\beta\sqrt{1+x^2-2x\cos\theta}\right]x^2dx\sin\theta d\theta \quad (5)$$
$$d\Omega=\sin\theta d\theta d\phi, x=r_n/r, dx=dr_n/r, \{r\equiv R_A, x'\equiv A/r\}$$

Substituting $u = [1+x^2 - 2x\cos\theta]^{1/2}$, $u\,du = x\sin\theta\,d\theta$ into the θ integration simplifies (5) to (6) and further reduces to (7) [12]:

$$2\pi r^3\int_0^{x'}xdx\int_{|1-x|}^{1+x}\exp\left[-j\beta u\right]du, \quad (6)$$

$$\pi r^3\int_0^{x'}xdx\left\{e^{\left(-j\beta(1+x)\right)\left[1+j\beta(1+x)\right]}-e^{\left(-j\beta|1-x|\right)\left[1+j\beta|1-x|\right]}\right\}\Big/\beta^2. \quad (7)$$

The final integration is divided into two regions due to the absolute value of (8) and reduces to (9) for $x' > 1$ and $\theta = \beta x'$:

$$\frac{\pi r^3}{\beta^2}\left(\begin{array}{l}\int_0^{1}xdx\left\{e^{\left(-j\beta(1+x)\right)\left[1+j\beta(1+x)\right]}-e^{\left(-j\beta|1-x|\right)\left[1+j\beta|1-x|\right]}\right\}+\\ \int_1^{x'}xdx\left\{e^{\left(-j\beta(1+x)\right)\left[1+j\beta(1+x)\right]}-e^{\left(-j\beta|1-x|\right)\left[1+j\beta|1-x|\right]}\right\}\end{array}\right), \quad (8)$$

$$\bar{F}_{x'>1}=4\pi j\left(r/\beta\right)^3e^{-j\theta}\left\{\begin{array}{l}2e^{j\theta}j\theta+\\ \left(1+j\theta-\theta^2/2\right)\left(\cos\beta-3\mathrm{sinc}\beta\right)+\\ \theta^2\left(\cos\beta-\mathrm{sinc}\beta\right)/2\end{array}\right\}. \quad (9)$$

For $x' < 1$ the term $|1 - x|$ simplifies to $(1 - x)$ and provides:

$$\bar{F}_{x'<1}=2\pi r^3\left(2je^{-j\beta}/\beta^3\right)\left\{\begin{array}{l}\sin\theta\left[\theta^2/\beta-j-3/\beta\right]+\\ \theta\cos\theta\left(j+3/\beta\right)\end{array}\right\}. \quad (10)$$

In the two-extremes of large and small x′, (10) reduces to (11) and (10) to (12), respectively:

$$\bar{F}_{x'\gg1}=6\sqrt{\left(\theta-\sin\theta\right)^2+\left(1-\theta^2/2-\cos\theta\right)^2}\Big/\theta^3, \quad (11)$$

$$\bar{F}_{x'\ll1}=\frac{-3\Psi\cos\left(\Psi\right)+3\sin\left(\Psi\right)}{\left(\Psi\right)^3}=3\mathrm{tinc}\left(\Psi\right), \quad (12)$$

where $\Psi = \theta = \beta x' = \beta A/r = k A$, is taken over all angular space (θ, ϕ). This validates Fig. 5 of [10] and yields a

Submitted On: October 1, 2018
Accepted On: October 20, 2018

graphical solution of 1.815, and agree with analysis provided in Fig. 3 of [2]. Expansions of this work in the Fresnel region were investigated in [5]–[6].[1]

We diverge by the approximation since we do not take an integral over the exact space of R_n, but its expansion of (1).

What is odd about this solution is the lack of pattern multiplication. No pattern multiplication exists due to a substitution from angular space to Ψ – space.

A sphere is composed of two symmetries a ball and a shell. The ball describes a azimuthal planar distribution in the x an y axes. The shell describes elevation symmetry in the z axis.

In addition, a sphere is composed of two types of symmetry a ball containing the interior of the sphere and rings comprising the outer shell of the sphere [5]–[10].

Compound random variables explains the true solution of a spherically distributed array. Pattern multiplication of the symmetries differs from historical works of [14]–[15]. We also note corrections to works of [3], [4] and [10] in Figs. 17–21 and Figs. 41–42 of [9].

A second method of deriving (12) is provided in [9] where integration of a plane wave is expanded as a sum of spherical waves in a spherically-symmetric volume:

$$\begin{aligned}&\frac{1}{V}\int_0^1\int_0^{2\pi}\int_0^{\pi} e^{j\vec{K}\cdot\vec{r}} = \frac{1}{V}\int_0^1\int_0^{2\pi}\int_0^{\pi} e^{jkAr(\hat{n}\cdot\hat{r})}\\ &= \frac{1}{V}\sum_{l=0}^{\infty}\int_0^1\int_0^{2\pi}\int_0^{\pi} (j)^l(2l+1)j_l(kr)P_l(\cos\psi)r^2\sin\theta d\theta d\phi\\ &V = 3/4\pi,\quad \vec{K} = kA\cos\psi,\ \cos\psi = (\hat{n}\cdot\hat{r})\\ &\hat{n} = \hat{r}(\theta_0,\phi_0) = \sin\theta_0\cos\phi_0\hat{x} + \sin\theta_0\sin\phi_0\hat{y} + \cos\theta_0\hat{z}\\ &\hat{r}(\theta,\phi) = \sin\theta\cos\phi\hat{x} + \sin\theta\sin\phi\hat{y} + \cos\theta\hat{z}.\end{aligned} \tag{13}$$

The spherical Hankel function of order zero h_0 (l=0) represents the spherically symmetric wave field. Hence, upon integration of a spherically uniform distribution one obtains the zeroth order mode:

$$\begin{aligned}&\frac{3}{4\pi}\int_0^1\int_0^{2\pi}\int_0^{\pi}(j)^0(2l+1)j_0(kAr)P_0(\cos\psi)r^2\sin\theta d\theta d\phi\\ &= 3\mathrm{Tinc}(kA).\end{aligned} \tag{14}$$

III. Mean Valued Radiation Pattern

The expected beampattern for any geometrically bound topology has been shown in [1] by taking the expected value of the array factor $|\bar{F}(\Psi)^2|$ across the unit interval [-1, 1]. Hence, for a volumetric random variable x this provides the characteristic functions (1), which are orthogonal in all three axes and uncorrelated. Hence, the analysis involves the characteristic functions of the aperture distribution [9], [10] and [14]:

$$\bar{U} = \frac{1}{N} + \left(1-\frac{1}{N}\right)\Lambda|u|^2\,\Lambda|v|^2\,\Lambda|w|^2 = \frac{1}{N} + \left(1-\frac{1}{N}\right)\Lambda|\vec{\Psi}|^2. \tag{15}$$

[1]Reciprocity applies to (12) such that the near field of a receiving array equals the far field of a transmit array.

The square magnitude of the characteristic function describes the main-lobe behavior of the array and, analysis of the radiation characteristics of random arrays relies on finding the characteristic functions of the aperture distribution. An example of (15) is applied to a spherical distribution of radiators as illustrated in Fig. 1. Verification of the pattern is obvious as a spherical distribution is remains consistency in its pattern behavior in both; θ and ϕ-cut planes and when scanned.

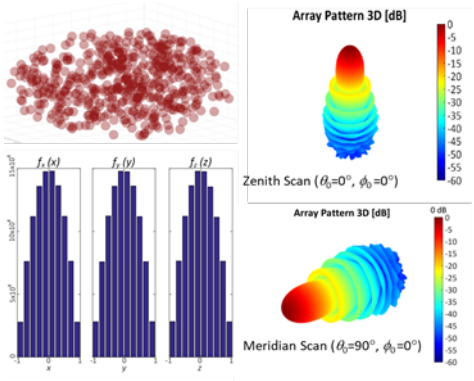

Fig. 1. Mean radiation pattern and cartesian coordinate distribution functions of a volumetric antenna array scanned from zenith to the meridian elevation angle.

IV. Physical Explanation

Taking the expected value of a random array is analogous to taking the average over all realizations of possible element placement. Mathematically, one may sample any topology using the inhomogeneous wave equation with point sources:

$$\nabla^2\psi + k^2\psi = \sum\delta\left(\vec{r} - \vec{r}_n'\right). \tag{16}$$

For the reference element the solution is:

$$\psi = \frac{e^{-jkr}}{4\pi r}. \tag{17}$$

Otherwise the solution becomes an offset from the origin as:

$$\psi = \sum_{n=1}^{N}\frac{e^{-jk|r-r_n|}}{4\pi|r-r_n|}. \tag{18}$$

The solution of (18) is approximated using a binomial expansion assuming equal path loss (19). For N elements, we find (20):

$$\psi = \sum_{n=1}^{N} e^{jkr_n(\cos\psi_n)}, \tag{19}$$

$$\psi \simeq \left(\frac{e^{-jkr}}{4\pi r}\right)\sum_{n=1}^{N} e^{jkr_n(\cos\psi_n)}, \cos\psi_n = \hat{r}_n\cdot\left(\hat{r}(\theta,\phi)\right). \tag{20}$$

The solution of the n^{th} element is out of phase by the angle ψ_n. Beamsteering is achieved by imposing the linear steering factor, cos ψ_{n0}. We obtain $e^{jkr_n(\hat{r}_n\cdot(\hat{r}(\theta,\phi)-\hat{r}(\theta_0,\phi_0)))}$. Upon phase

correction these sources are now isotropic with equal amplitudes and propagate waves that intersect at alternating maxima and minima as shown in Fig. 2. A Fourier Transform pair describes the superposition of the constructive destructive interference of the particle nature of the wave, which is easy to visualize in the Fraunhofer region.

As the number of sources grows to infinity ($N\to\infty$) the discrete pattern converges to a continuous aperture solution. However, when N does not approach infinity the solution is the expected value and is illustrated in Fig. 3. The difference in relations yields a convergence factor of ($1/N$) between the aperiodic array and continuous aperture where the former is the characteristic function on a pedestal ($1/N$).

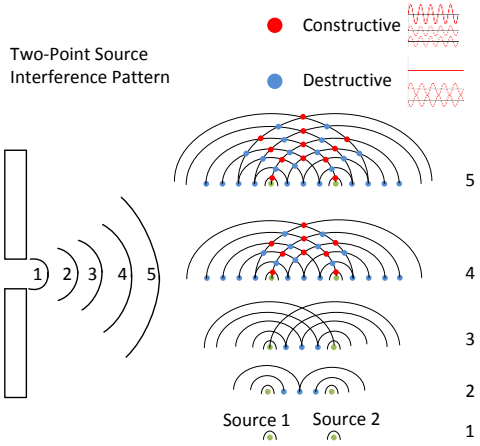

Fig. 2. Representation of constructive and destructive interference.

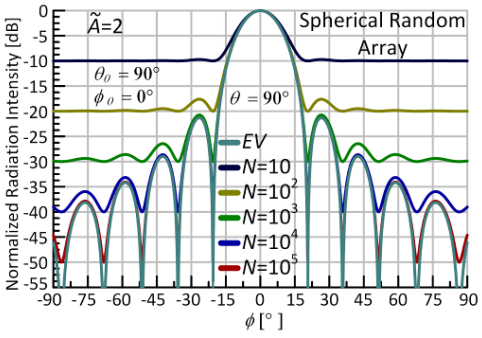

Fig. 3. Superposition diagram (top) converges to a continuous aperture distribution (*EV*) as $N\to\infty$ (bottom).

A. Spherical Waves in Unbounded Space

The characteristic modes of the spherical harmonics are derived from the fundamental solution of the Helmholtz equation (21) in unbounded space,

$$\left(\nabla^2+k^2\right)G_k=-\delta\left(\vec{r}-\vec{r}\,'\right)=-\frac{\delta\left(r-r'\right)\delta\left(\theta-\theta'\right)\delta\left(\phi-\phi'\right)}{rr'\sin\theta} \quad (21)$$

$$G_k\left(\vec{r},\vec{r}\,'\right)=G_k\left(\vec{r}-\vec{r}\,'\right)=jh_0^{(1)}\left(jk\left|r-r'\right|\right)/4\pi=G_k\left(\vec{r}\,',\vec{r}\right)$$

Thus, the fundamental solution (21) is a point source and implies the self-adjointness property such that $G_k\left(\vec{r},\vec{r}\,'\right)=G_k\left(\vec{r}\,',\vec{r}\right)$. In other words, a spherical wave converges to a plane wave in the far field and vice versa.

An expansion of (21) as a scalar plane wave composed of scalar spherical waves can also be written as (22). From the orthogonality property of the spherical harmonics, outgoing waves are composed from multipole coefficients derived from the pattern multiplication of spherical Hankel, Bessel and spherical harmonics (23):

$$G\left(\vec{r}_1,\vec{r}_2\right)=jk\sum_{l=0}^{\infty}\begin{Bmatrix} j_l\left(kr_1\right)h_l^{(1)}\left(kr_2\right)\ \left[r_1<r_2\right] \\ j_l\left(kr_2\right)h_l^{(1)}\left(kr_1\right)\ \left[r_1>r_2\right]\end{Bmatrix}\sum_{m=-l}^{l}Y_l^m\left(\theta_1,\phi_1\right)Y_l^{m*}\left(\theta_2,\phi_2\right), \quad (22)$$

$$G\left(\vec{r},\vec{r}\,'\right)=jk\sum_{l=0,\infty}j_l\left(kr_<\right)h_l^{(1)}\left(kr_>\right)\sum_{m=-l,+l}Y_{lm}^*\left(\theta',\phi'\right)Y_{l,m}\left(\theta,\phi\right)$$

$$-\oint Y_{lm}^*\left(\theta,\phi\right)G\left(\vec{r},\vec{r}\,'\right)d\Omega=jkh_l^{(1)}\left(kr\right)j_l\left(kr'\right)Y_{lm}^*\left(\theta',\phi'\right) \quad (23)$$

In the far field the term $|\vec{r}-\vec{r}\,'|\approx r'-\vec{n}\cdot\vec{r}$, where $\vec{n}$ is a unit vector pointing in the direction of $\vec{r}\,'$. $h_l^{(1)}\left(kr\right)$ can be reduced in its asymptotic form such that:

$$\frac{e^{j\vec{k}\cdot\vec{r}}}{4\pi r}e^{-j\vec{k}\cdot\vec{r}\,'}=jk\frac{e^{jkr}}{kr}\sum_{l=0}^{\infty}\left(-j\right)^{l+1}j_l\left(kr'\right)\sum_{m=-l,+l}Y_{lm}^*\left(\theta',\phi'\right)Y_{l,m}\left(\theta,\phi\right) \quad (24)$$

The scalar plane wave expansion (25) is obtained by canceling the factor $\exp(jkr)/r$, taking the complex conjugate, and rewriting via the well-known addition theorem (26):

$$e^{j\vec{k}\cdot\vec{r}\,'}=4\pi\sum_{l=0}^{\infty}j^l j_l\left(kr'\right)\sum_{m=-l,+l}Y_{lm}^*\left(\theta',\phi'\right)Y_{l,m}\left(\theta,\phi\right), \quad (25)$$

$$e^{j\vec{k}\cdot\vec{r}\,'}=\sum_{l=0}^{\infty}j^l\left(2l+1\right)j_l\left(kr'\right)P_l\left(\cos\psi\right)$$

$$=\sum_{l=0}^{\infty}j^l\sqrt{4\pi\left(2l+1\right)}j_l\left(kr'\right)Y_{l0}\left(\psi\right), \quad (26)$$

$$Y_{l0}\left(\psi\right)=P_l\left(\cos\psi\right)\sqrt{\left(2l+1\right)/4\pi},\psi=\hat{r}\cdot\hat{r}\,'$$

Higher order moments do contribute to our overall pattern, but have a neglible impact.

B. Zernike Polynomials and Spherical Harmonics

It is possible to create patterns with multiple beams using complex orthogonal phase variations. A nominal example in *UV-space* is provided in Fig. 4.

Distributed orthogonality of this behavior is applied to the plane wave expansion of ψ and angular (θ, ϕ) spaces of Fig. 5 and Fig. 6, respectively. Fig. 5 demonstrates *ψ-spaces* with rotationally symmetric attributes, whereas Fig. 6 demonstrates the self-adjoint properties of spherically distributed arrays (SDA). For example, a spherical wave converges to a plane wave as the modal order increases while the point source converges to a spherical wave.

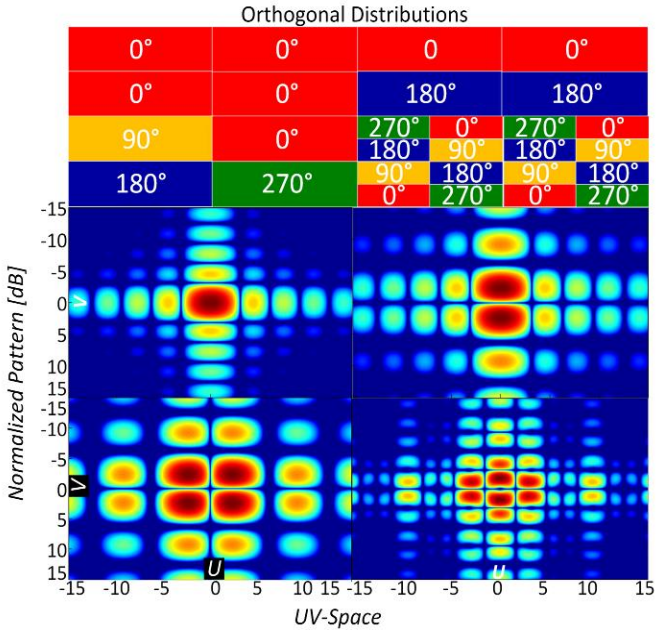

Fig. 4. Multiple beam patterns and distributed orthogonality.

The Legendre polynomials, which are orthogonal to the L^2 inner product on the interval $-1 \le x \le 1$, are the eigenfunctions of the Hermitian differential operator. They arise naturally in multipole expansions analogous to the monopole, dipole and higher moments of the spherical harmonic solutions, yielding the beampattern characteristics in Fig. 7. Furthermore, achievable pattern behavior is verified from HFSS simulations using 32 monopole element radiators steered at the meridian elevation angle in a normalized spherical aperture, A/λ=2.78 for select orbital distributions.

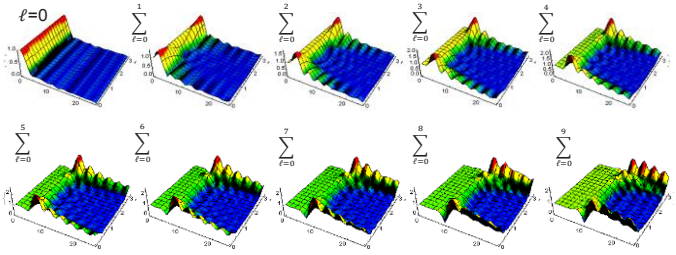

Fig. 5. Plane wave expansion in UV – space.

The three-dimensional Zernike polynomials are likewise composed of angular solutions of an orthogonal sequence defined on the unit sphere. In two-dimensional space, Zernike polynomials are commonly used in optics to describe aberrations of the cornea or lens from the nominal spherical shape (resulting in refraction errors). Examples include a circularly distributed array (CDA) as illustrated in Fig. 7. Closed form solutions of the patterns are provided in [9]. Lastly, they can represent properties of an image with no overlap of information between their moments as illustrated by Fig. 8. A final illustration of the beampatterns generated from the atomic like orbitals is shown in Fig. 9 as these distributions apply to the spherical zone of probability describing an electron's location.

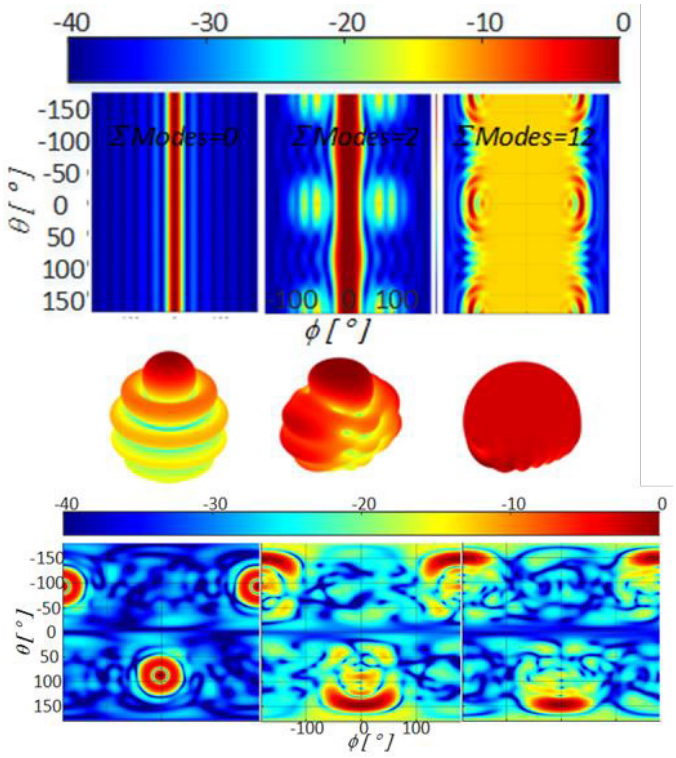

Fig. 6. Comparison of the modal summation of (25) applied to a point source in angular space, top and SDA, bottom.

V. Conclusion

The decomposition of (21) can be used to obtain the individual moments of the field at a given distance away from the source. These solutions formulate a series of basis functions for determining the array factor such that:

1. Monopole moments in the Fraunhofer region ($R>2D^2/\lambda$);
2. Monopole + Dipole moments in the Fresnel region with the first two spherical Hankel functions;
3. Monopole + Dipole + Quadrupole + Higher order modes in the near reactive field region;

and for a spherically distributed antenna array we reduce the number of basis functions of the pyramid of Fig. 8 and apply the spherical addition theorem (n as the n^{th} element) by:

$$P_l\left(\cos\psi = \hat{r}\cdot\hat{r}_n\right) = \frac{4\pi}{2l+1}\sum_{m=-l}^{l} Y_{lm}^{*}\left(\theta_n,\phi_n\right)Y_{lm}\left(\theta_{n0},\phi_{n0}\right). \quad (27)$$

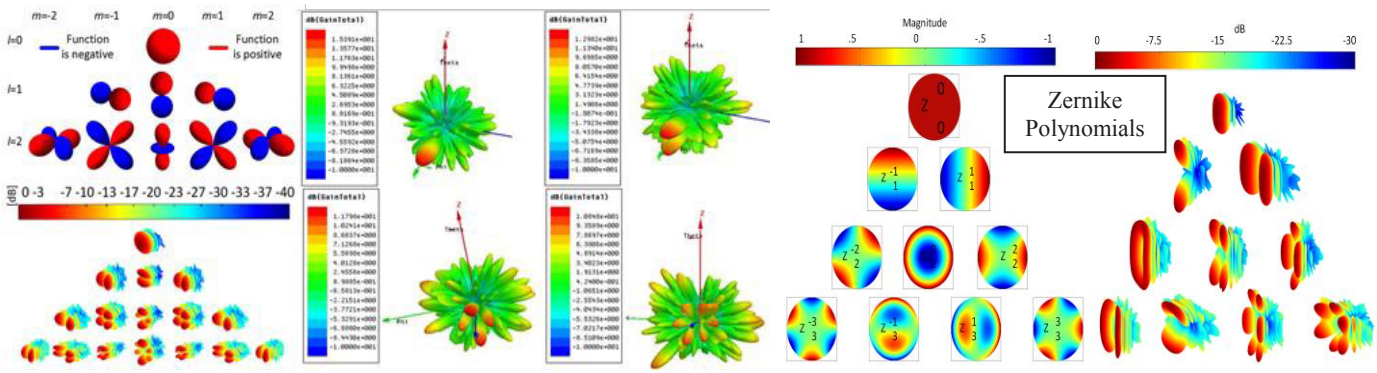

Fig. 7. Spherical harmonic distributions $Y_{mn,}$ top-left; modal beampatterns bottom-left; simulated patterns Y_{00}, Y_{01}, Y_{02}, and Y_{03}, center; Zernike distributions and modal beampatterns right.

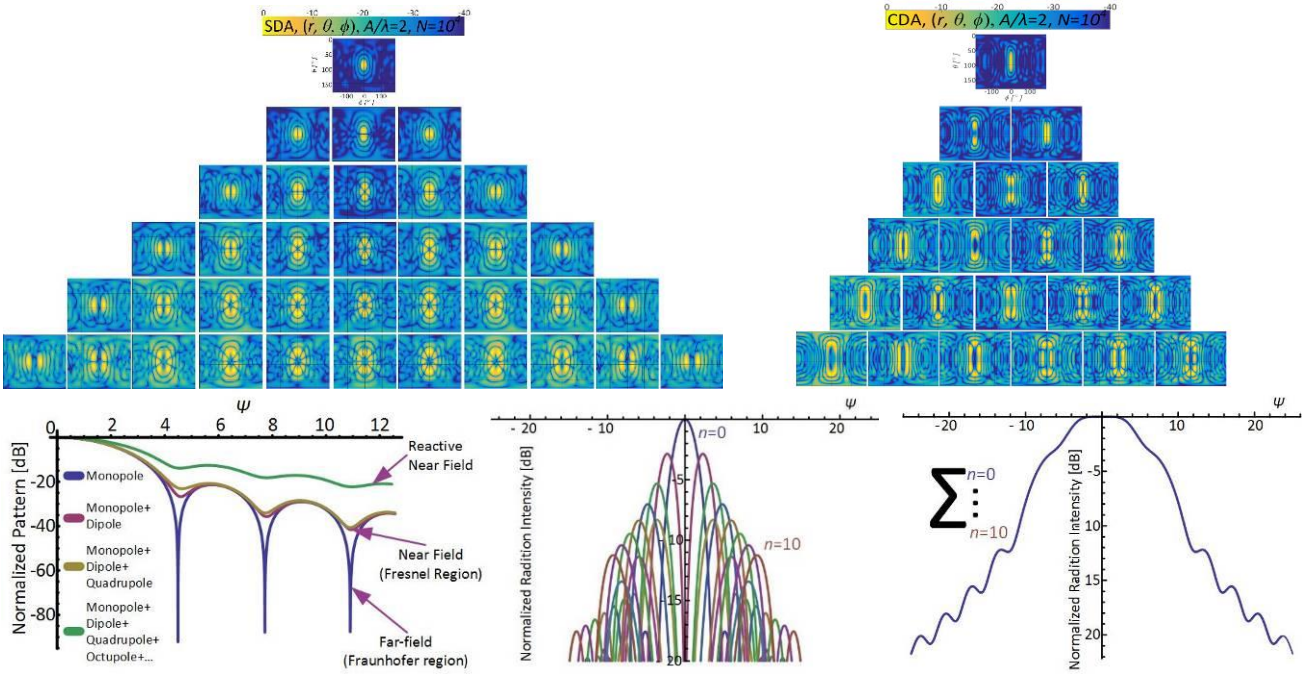

Fig. 8. Characteristic modes of the Zernike and spherical harmonic polynomials; topographical – top. Atomic orbital relationship of the superposition of spherical waves to a plane wave (bottom left). Zernike descending characteristic functions (bottom middle), characteristic function superposition (bottom right).

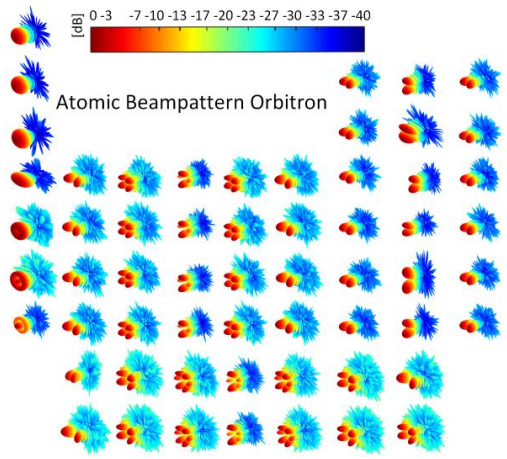

Fig. 9. Atomic like orbital beampatterns.

REFERENCES

[1] A. Panicali and L. Yuen, "A probabilistic approach to large circular and spherical arrays," IEEE Trans. Antennas Propag., vol. 17, pp. 514-522, July 1969.

[2] T. A. Dzekov and R. S. Berkowitz, "Parameters of a spherical random antenna array," in Electron. Lett., vol. 14, no. 16, pp. 495-496, Aug. 1978.

[3] H. Ochiai, "Collaborative beamforming for distributed wireless ad hoc sensor networks," IEEE Trans. Signal Process., vol. 53, pp. 4110, Nov. 2005.

[4] M. F. A. Ahmed and S. A. Vorobyov, "Collaborative beamforming for wireless sensor networks with Gaussian distributed sensor nodes," IEEE Trans. on Wireless Commun., vol. 8, pp. 638-643, Feb. 2009.

[5] K. Buchanan, O. Sternberg, S. Wheeland, and J. Rockway, "Examination of the near field response of circular antenna arrays," in United States National Committee of URSI National Radio Science Meeting (USNC-URSI NRSM), Boulder, CO, Jan. 2017, pp. 1-2.

[6] K. Buchanan, C. Flores-Molina, O. Sternberg, D. Overturf, S. Wheeland, and N. Johnson, "Near-field receive beamforming analysis

using circularly distributed random arrays," in IEEE Antennas and Propag. Int. Symp., San Diego, CA, 2017, pp. 1591-1592.

[7] D. Overturf, K. Buchanan, J. Jensen, C. Flores-Molina, S. Wheeland and G. H. Huff, "Investigation of beamforming patterns from volumetrically distributed phased arrays," in IEEE Military Communications Conference (MILCOM), Baltimore, MD, Oct. 2017, pp. 817-822.

[8] K. Buchanan and G. Huff, "A comparison of geometrically bound random arrays in Euclidean space," in IEEE Antennas and Propag. Soc. Int. Symp., Spokane, WA, July 2011, pp. 3-8.

[9] K. R. Buchanan, "Theory and applications of aperiodic (random) phased arrays," Ph.D. dissertation, Dept. Elect. & Com. Eng., Texas A&M University, TX, 2014.

[10] K. Buchanan and G. Huff, "A stochastic mathematical framework for the analysis of spherically bound random arrays," IEEE Trans. Antennas Propag., vol. 62, pp. 3002-3011, June 2014.

[11] D. Yavuz, "Frequency response and bandwidth of a spherical random array," in Electron. Lett., vol. 15, no. 11, pp. 314-315, May 1979.

[12] L. Lewin, "Comment analytic expression for the frequency response and bandwidth of a spherical random array," in Electron. Lett., vol 15. no. 19, pp. 585-586, Sept. 1979.

[13] K. Buchanan, C. Flores, S. Wheeland, J. Jensen, D. Grayson, and G. Huff, "Transmit beamforming for radar applications using circularly tapered random arrays," in IEEE Radar Conference (RadarConf), Seattle, WA, 2017, pp. 0112-0117.

[14] B. D. Steinberg, Principles of Aperture & Array System Design. New York: Wiley, 1976.

[15] Y. Lo, "A mathematical theory of antenna arrays with randomly spaced elements," IEEE Trans. Antennas Propag., vol. 12, pp. 257-268, May 1964.